

## Multiple Rotational Doppler Effect Induced by a Single Spinning Meta-Atom

Jun Luo<sup>1,2</sup>, Yuhui Wang,<sup>1,2</sup> Mingbo Pu<sup>1,2,3,\*</sup>, Fei Zhang,<sup>1,2,3</sup> Mingfeng Xu,<sup>1,2,3</sup> Xiaoliang Ma,<sup>1,2</sup> Xiong Li,<sup>1,2</sup> Cheng Huang,<sup>1,2</sup> Zuojun Zhang,<sup>1,2</sup> Lianwei Chen,<sup>1,3</sup> and Xiangang Luo<sup>1,2,†</sup>

<sup>1</sup>*State Key Laboratory of Optical Technologies on Nano-Fabrication and Micro-Engineering, Institute of Optics and Electronics, Chinese Academy of Sciences, Chengdu 610209, China*

<sup>2</sup>*School of Optoelectronics, University of Chinese Academy of Sciences, Beijing 100049, China*

<sup>3</sup>*Research Center on Vector Optical Fields, Institute of Optics and Electronics, Chinese Academy of Sciences, Chengdu 610209, China*

(Received 2 November 2022; revised 28 February 2023; accepted 14 March 2023; published 21 April 2023)

The rotational Doppler effect (RDE) is of fundamental importance in the detection of rotating systems, ranging from molecules to macroscopic bodies. Metasurfaces, which are potential substitutes for traditional optical devices, have been reported to induce a RDE. However, the mechanism of the interaction between an electromagnetic wave and a spinning artificial meta-atom is not yet fully understood. Here, we report a multiple RDE based on a time-varying generalized Pancharatnam-Berry phase, obtained from a single spinning meta-atom placed in a rectangular waveguide. Twofold and sixfold rotational Doppler shifts with respect to the rotational velocity are obtained from meta-atoms with C2 and C3 rotational symmetry, respectively. In contrast to full-size devices, a single meta-atom has minimal rotational inertia and size, enabling its application in integrated systems. This work represents the interaction of an electromagnetic wave with a single spinning meta-atom, which may have potential applications in rotation-detection systems, frequency-gradient metasurfaces, and frequency modulators.

DOI: 10.1103/PhysRevApplied.19.044064

### I. INTRODUCTION

The translational Doppler effect is the well-known frequency shift of electromagnetic or sound waves that arises from relative motion between the source and the detector [1,2]. This frequency shift is proportional to both the frequency of the wave source and the linear velocity, and has been successfully applied for measurement of the speed and position of objects in medical diagnosis [3], global positioning systems [4], and Doppler radar [5]. Similarly to the translational Doppler effect, the rotational Doppler effect is derived from the exchange of angular momentum and energy when electromagnetic waves carrying angular momentum interact with rotating objects [6]. This phenomenon can be observed in the case of a circularly polarized (CP) wave propagating through a gas of synchronously spinning molecules [7]. This effect can be employed to measure the angular velocity and angular acceleration of an object using the rotational-Doppler-shift information in the echo signal [8–10]. There are three main ways to induce a rotational Doppler frequency shift. The typical way is to use a CP wave carrying spin angular momentum (SAM), which propagates through one or

two cascaded spinning half-wave plates with an angular velocity  $\Omega$ ; the output CP wave with opposite handedness experiences an angular-frequency shift of  $2\Omega$  or  $4\Omega$  [11,12]. To increase the frequency shift, light beams carrying both SAM and orbital angular momentum (OAM) have been produced by utilizing a spatial light modulator (SLM) or a spiral phase plate [13–17]. In addition, a spinning nonlinear crystal has been introduced to induce a rotational Doppler effect (RDE), which provides an insight into the interaction of light with a moving medium in the nonlinear optical regime [18]. However, such methods suffer from the limitations of complicated optical elements and low efficiency due to the divergence of a beam with OAM in free space.

Metasurfaces, which are artificially designed materials, offer an unprecedented ability to manipulate the polarization, phase, and amplitude of electromagnetic waves [19–25]. Spinning  $q$ -plates consisting of a metasurface with a low profile thickness can be used to replace traditional optical elements (SLMs, spiral phase plates, and spinning half-wave plates) and to generate an OAM that can induce a rotational Doppler frequency shift under illumination with a CP wave [26–28].

In addition, time-modulated metasurfaces based on varactor diodes or PIN diodes have been demonstrated to achieve a RDE when the bias voltages are controlled

\*Corresponding author. pmb@ioe.ac.cn

†Corresponding author. lxg@ioe.ac.cn

[29–31]. Therefore, a RDE generated by a rotating meta-surface can be used to cloak the motion of a moving object from an observer by compensating for the translational Doppler shift [32]. Similarly, the RDE can be expanded to the field of acoustics and can be used to generate acoustic folded bulk bands and interface-state bands based on acoustic array metasurfaces [33]. More recently, the use of the generalized Pancharatnam-Berry (PB) phase based on polygonal meta-atoms with high rotational symmetries has been proposed for realizing an on-demand phase for OAM generation and beam deflection [34,35]; this violates the well-known theory that a geometric phase does not exist for meta-atoms with a rotational symmetry greater than or equal to 3 [36]. Interestingly, a single meta-atom with a generalized PB phase, with minimal rotational inertia and size, is expected to induce a Doppler frequency shift, which could potentially lead to a broad range of applications, especially in integrated systems.

In this paper, we focus on the RDE of a single spinning meta-atom with high rotational symmetry. Theoretical analysis demonstrates that a RDE can originate from a time-varying PB phase in a symmetric meta-atom structure. It is shown that the absolute rotational Doppler shift depends not only on the rotational speed but also on the rotational symmetry of the meta-atom structure. The time-varying polarization conversion efficiency and PB phase are measured in a microwave waveguide experiment. We successfully observe twofold (C2 meta-atom) and sixfold (C3 meta-atom) rotational Doppler shifts with respect to the rotation speed. The rotational symmetry of a single meta-atom, which offers a degree of freedom for frequency-shift modulation, expands and enriches the theory of the RDE. More essentially, this demonstration is of fundamental significance in electromagnetics and photonics, as it provides insight into the interaction of an electromagnetic wave with a single spinning meta-atom with high symmetry.

## II. THEORETICAL ANALYSIS AND META-ATOM DESIGN

The high-order PB phase induced by a meta-atom with  $n$ -fold rotational symmetry in a square lattice can be expressed as [34]

$$\Phi(n) = \begin{cases} \pm 2n\theta, & n \text{ odd} \\ \pm n\theta, & n \text{ even} \end{cases} \quad (n \neq 4m, m = 1, 2, 3, \dots), \quad (1)$$

where the sign  $\pm$  is determined by the rotation direction of the principal axis, and  $\theta$  is the rotation angle with respect to the principal axis of the meta-atom. The generalized PB phase is manifested as a multiple-times rotation angle different from the usual geometric phase  $\Phi = \pm 2\theta$ . We analyze the relationship between the rotational Doppler shift and the generalized PB phase for an

electromagnetic wave interacting with a spinning object. Assuming that a wave with a right-handed circular polarization (RCP) or left-handed circular polarization (LCP)  $E_i = E_0 \exp[-i(\omega t - kz)] \left[ \begin{smallmatrix} 1 \\ \pm i \end{smallmatrix} \right]$  impinging on a reflecting interface is completely converted to a CP wave with the same handedness, the detected echo signal can be written as

$$E_R = E_1 \exp\{i[\omega t - kz - \Psi[r(t)]]\} \left[ \begin{smallmatrix} 1 \\ \pm i \end{smallmatrix} \right], \quad (2)$$

where  $E_0$  and  $E_1$  are the amplitudes of the incident electromagnetic wave and of the echo signal at the detector;  $\omega$ ,  $k$ , and  $r$  are the angular frequency, the wave vector, and the transverse position across the wavefront of the electromagnetic wave; and  $\Psi[r(t)]$  is the transverse phase of the reflected wave. The longitudinal phase is determined by the propagation distance  $z$ . For a single  $n$ -fold-symmetric meta-atom spinning at an angular velocity  $\Omega$  in a square lattice, the transverse phase  $\Psi[r(t)]$  is equal to the PB phase of the meta-atom  $\Phi(n, t)$ , which is independent of the transverse position  $r$ . According to Eq. (1), the time-varying PB phase of a meta-atom with  $n$ -fold rotational symmetry is given by

$$\Phi(n, t) = \begin{cases} \pm 2n\Omega t, & n \text{ odd} \\ \pm n\Omega t, & n \text{ even} \end{cases} \quad (n \neq 4m, m = 1, 2, 3, \dots), \quad (3)$$

where the rotation angle of the meta-atom is expressed as  $\theta = \Omega t$ . We define the time-varying phase of the echo signal in Eq. (2) as  $\chi = \omega t - kz - \Psi[r(t)]$ . Considering only the rotation of the meta-atom, the total phase-change rate of the reflected echo signal can be written as [37]

$$\frac{\partial \chi}{\partial t} = \omega - \frac{\partial \Psi[r(t)]}{\partial t}. \quad (4)$$

According to Eqs. (3) and (4), we obtain a rotational Doppler frequency shift that can be expressed as

$$\Delta\omega = \frac{\partial \Psi[r(t)]}{\partial t} = \frac{\partial \Phi(n, t)}{\partial t} = \begin{cases} \pm 2n\Omega, & n \text{ odd} \\ \pm n\Omega, & n \text{ even} \end{cases} \quad (n \neq 4m, m = 1, 2, 3, \dots), \quad (5)$$

where the sign  $\pm$  is determined by both the rotation direction of the principal axis and the handedness of the circular polarization of the incident wave. In other words, the angular frequency is either downshifted or upshifted, corresponding to either a parallel and/or an antiparallel rotation between the meta-atom and the spin angular momentum of the incident CP wave. From the above analysis, we can see that a multiple RDE originates from the generalized PB

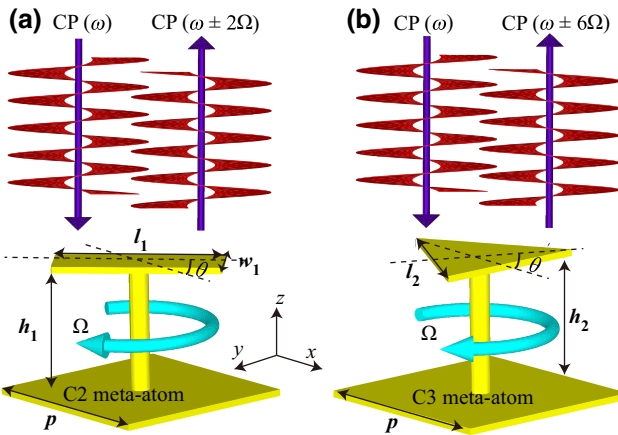


FIG. 1. Schematic diagrams of RDE for C2 and C3 meta-atoms. The incident CP wave is reflected and converted from a CP wave with the same handedness by C2 and C3 meta-atoms with angular velocity  $\Omega$ , and the reflected wave has absolute rotational Doppler shifts of  $2\Omega$  and  $6\Omega$  (angular frequency), respectively. (a) Geometrical parameters of C2 rectangular meta-atom:  $p = 20$  mm,  $l_1 = 18$  mm,  $w_1 = 5$  mm, and  $h_1 = 7.5$  mm. (b) Geometrical parameters of C3 equilateral-triangular meta-atom:  $p = 20$  mm,  $l_2 = 15.89$  mm, and  $h_2 = 6.5$  mm.

phase when that phase is equal to several times the rotation angle with respect to the principal axis of the meta-atom. Hence, the absolute rotational Doppler shift depends not only on the angular velocity  $\Omega$  but also on the  $n$ -fold rotational symmetry. We have analyzed the Jones matrix of the multiple RDE for a CP incident wave interacting with a spinning object with  $n$ -fold symmetry (see Sec. S1 in the Supplemental Material [38]).

Diagrams of the RDE for C2 and C3 meta-atoms according to the above theoretical analysis are shown in Figs. 1(a) and 1(b), respectively. For the usual rectangular meta-atom with twofold rotational symmetry and with an angular velocity  $\Omega$ , an incident LCP (or RCP) wave can be reflected and converted to a LCP (or RCP) wave with the same handedness, which generates a rotational Doppler shift of  $2\Omega$  (or  $-2\Omega$ ) and  $-2\Omega$  (or  $2\Omega$ ) for the clockwise and the anticlockwise rotation direction, respectively. Differently from a C2 meta-atom, a LCP (or RCP) wave reflected from a C3 equilateral-triangular meta-atom can carry a rotational Doppler shift of  $6\Omega$  (or  $-6\Omega$ ) and  $-6\Omega$  (or  $6\Omega$ ) for the clockwise and the anticlockwise rotation direction, respectively. To verify the existence of a multiple RDE induced by the generalized PB phase, we design all-metal meta-atoms with C2 and C3 rotational symmetry, and the corresponding geometrical parameters are shown in Figs. 1(a) and 1(b), respectively. Microwave waveguide devices and a stepping motor are used to measure the time-varying polarization conversion and generalized PB phase induced by a single spinning meta-atom placed in a rectangular waveguide.

### III. EXPERIMENTAL RESULTS

#### A. Generalized PB phase

A schematic illustration of the waveguide devices used experimentally for measuring the polarization conversion efficiency and PB phases of spinning meta-atoms is shown in Fig. 2(a). An orthogonal-mode transducer is used to separate two orthogonal linearly polarized signals within the same frequency band. A circular-polarizer waveguide acts as a polarization converter between linearly polarized (LP) and CP waves. When the input signal to port 1, provided by a vector network analyzer, passes through the OMT, the output LP wave from the common port of the OMT is converted into a CP wave by the CPW. The rectangular-circular waveguide plays an important role in the junction between the rectangular port of RW and the circular port of CPW. Without a meta-atom, the reflecting waveguide converts the CP wave into one with the opposite circular polarization, due to half-wave loss. Then, the CP wave with opposite handedness, after passing through the CPW, is converted into one with a linear polarization orthogonal to that of the incident polarized wave (the input signal to port 1), and the orthogonal linear polarization is received by port 2 ( $S_{21,1}$ ) through the OMT. When a meta-atom is installed, the CP wave can be transformed into a CP wave with the same handedness under the action of a reflective meta-atom, because the meta-atom can be considered as a half-wave plate. Thus, this same-handedness CP wave can be converted into one with a linear polarization parallel to that of the incident LP wave (the input signal to port 1) after passing through the CPW, and then the linear polarization separated by the OMT is received at port 1 ( $S_{11}$ ). In other words, the portion of the electromagnetic wave that has undergone polarization conversion by the meta-atom returns to port 1 ( $S_{11}$ ), and another portion of the electromagnetic wave, without polarization conversion by the meta-atom, is received at port 2 ( $S_{21,2}$ ). Note that the meta-atom sample is fixed to the shaft of the motor, which passes through a small hole in the reflecting waveguide. Electromagnetic absorption can be ignored, due to the all-metal structure. As a result, the polarization conversion efficiency  $\eta$  can be indirectly obtained from  $\eta = S_{21,1} - S_{21,2}$ , where  $S_{21,1}$  and  $S_{21,2}$  are the output signals from port 2 for the unloaded sample and for the sample loaded with a meta-atom, respectively. As the signal  $S_{11}$  carries information about the absolute amplitude of the polarization conversion and the phase, the PB phase can also be measured by collecting phase information from  $S_{11}$  when the meta-atom structure is rotated at a lower speed. We have given a Jones-matrix-theory analysis of the polarization conversion and PB phase in waveguide devices (see Sec. S2 in the Supplemental Material [38] for more details).

For convenient acquisition of the variation with time or rotation angle of the polarization conversion efficiency and

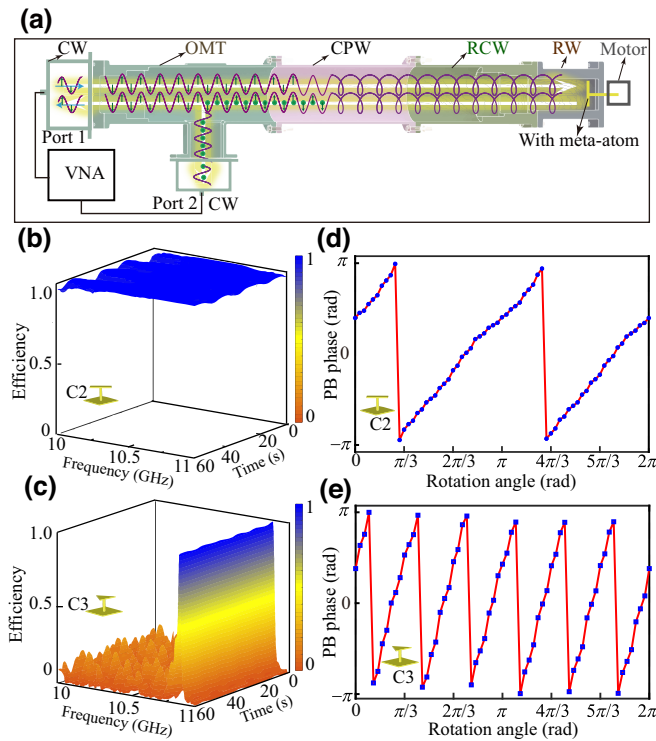


FIG. 2. Experimental setup and measurement results obtained from samples with C2 and C3 meta-atoms. (a) Experimental setup, consisting of a vector network analyzer (VNA), two coaxial-to-waveguide (CW) adapters, an orthogonal-mode transducer (OMT), a circular-polarizer waveguide (CPW), a rectangular-circular waveguide (RCW), a reflecting waveguide (RW), and a motor, connected in sequence. (b),(c) Variation of measured polarization conversion efficiency of C2 meta-atom with frequency and time. (d),(e) Variation of measured PB phase of C2 and C3 meta-atoms with rotation angle, corresponding to frequencies of 10.5 and 10.85 GHz.

PB phase of a meta-atom, we set a lower angular velocity  $\Omega = 0.03\pi$  rad/s. The measured polarization conversion efficiency of the C2 and C3 meta-atoms varies with frequency and time, as shown in Figs. 2(b) and 2(c). The results demonstrate that the polarization conversion efficiency of meta-atoms with different rotational symmetry remains almost unchanged at any time when the meta-atom structure is rotated. The polarization conversion efficiency of the C2 meta-atoms exceeds 95% in the frequency range from 10 to 11 GHz. Although Fig. 2(c) demonstrates the narrow-band polarization conversion efficiency of a C3 triangular meta-atom, the maximum of the reflection efficiency is close to 100% at a frequency of 10.85 GHz. PB-phase envelopes for different times in the frequency range from 10 to 11 GHz can be seen in Fig. S2 in the Supplemental Material [38]. It can be seen that the PB phase of the C2 meta-atom completely covers the full phase range of  $2\pi$  in the frequency range from 10 to 11 GHz, but the PB phase of the C3 meta-atom covers the  $2\pi$  phase range

only in the frequency range from 10.5 to 10.9 GHz. The PB phases of the C2 rectangular (10.5 GHz) and C3 triangular (10.85 GHz) meta-atoms vary with the rotation angle, as shown in Figs. 2(d) and 2(e). The PB phase of the C2 rectangular meta-atom is twice the rotation angle. In sharp contrast to the C2 meta-atom, the PB phase of the C3 meta-atom is six times the rotation angle. The measured PB phases of the C2 and C3 meta-atoms are consistent with the theoretical expectations from Eq. (1). By employing our waveguide devices and a single meta-atom, we can measure the time-varying PB phase. This is helpful for reducing the cost of fabrication and avoiding full-size samples. In addition, measurement results for a C3 Y-shaped meta-atom are demonstrated in Sec. S3 in the Supplemental Material [38]. By comparing the measurement results for the triangular and Y-shaped meta-atoms, we find that these two meta-atoms with the same rotational symmetry have similar electromagnetic properties in terms of the polarization conversion and PB phase.

## B. Rotational Doppler frequency shift

To further determine the multiple RDE of meta-atoms with  $n$ -fold rotational symmetry, another experiment is performed, in which the rotation speed of a single meta-atom is controlled with a stepper motor. A schematic diagram of the experimental setup is shown in Fig. 3(a), where a signal source (Keysight N5191A) and a spectrum analyzer (R&S FSW) are utilized to generate input pulse signals and receive echo signals, respectively. To improve the resolution of the frequency acquisition, we need to use a modulated narrow pulse as the incident signal, as shown in Fig. 3(b) (see Sec. S4 in the Supplemental Material [38] for details of the tests and theoretical analysis).

Spectra measured for the C2 and C3 meta-atoms with different angular velocities  $\Omega$  in the clockwise direction are shown in Figs. 3(c)–3(h), indicating the symmetric characteristics of the right and left sides with respect to the center modulation frequency. The main peaks on the right and left sides correspond to the rotational frequency shifts of the LCP and RCP components. After they have been reflected by the rotating C2 rectangular meta-atom, the two CP waves experience opposite rotational frequency shifts of  $\pm 2\Omega$  rad/s. When the C2 rectangular meta-atom is rotated, the main peaks in Figs. 3(c)–3(e) illustrate the rotational frequency shifts  $\Delta f = \pm 35.96, \pm 53.95$ , and  $\pm 71.93$  Hz obtained when clockwise angular velocities  $\Omega = 18 \times 2\pi, 27 \times 2\pi$ , and  $36 \times 2\pi$  rad/s, respectively, are chosen. This indicates that the rotational frequency shift (angular frequency) for the C2 meta-atom is twice the rotation speed. For the C3 triangular meta-atom with clockwise angular velocities  $\Omega = 18 \times 2\pi, 27 \times 2\pi$ , and  $36 \times 2\pi$  rad/s, rotational frequency shifts  $\Delta f = \pm 107.89, \pm 161.84$ , and  $\pm 215.87$  Hz, respectively, are observed in Figs. 3(f)–3(h). The rotational frequency shift (angular frequency) for the

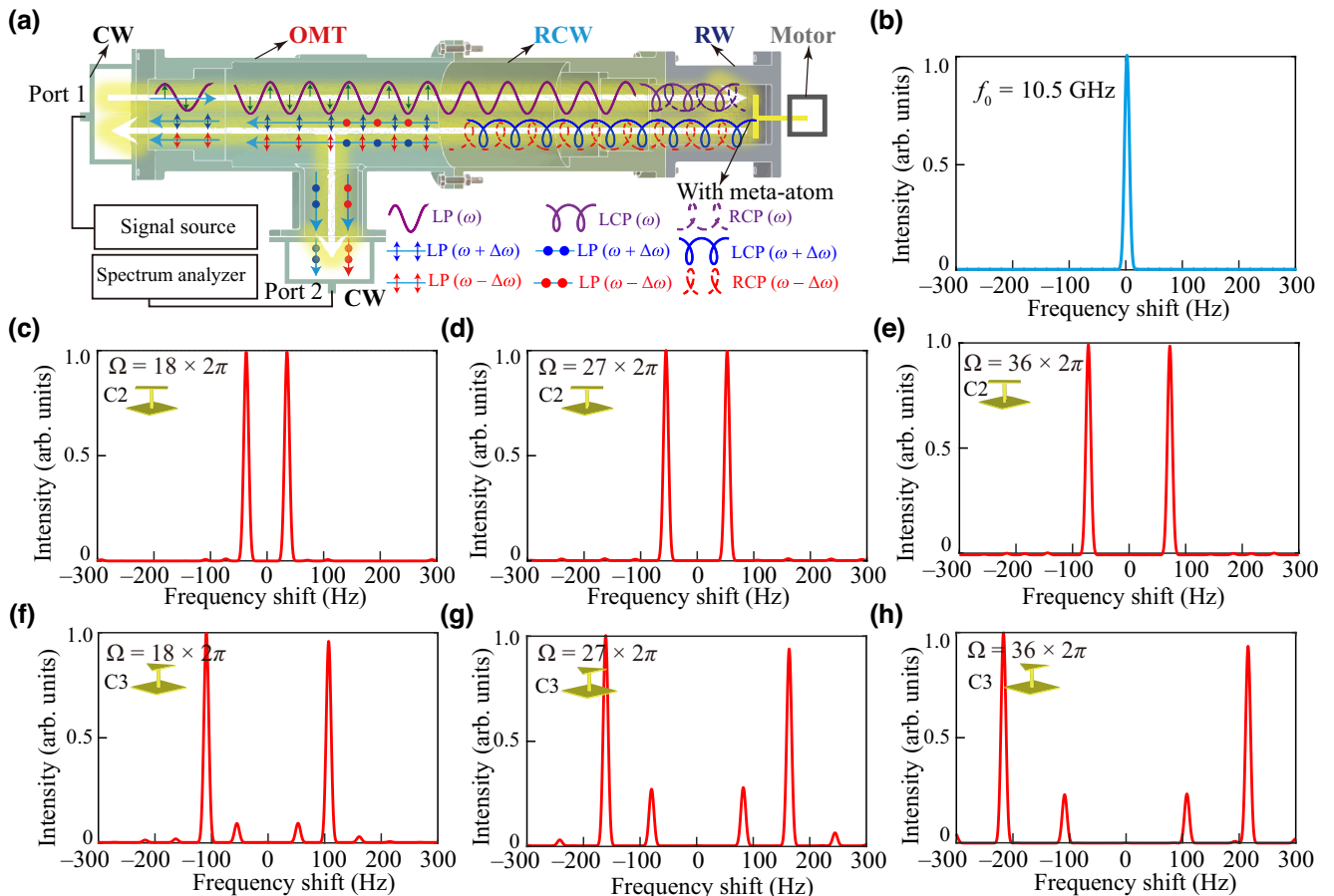


FIG. 3. Experimental setup and measurement results for the rotational frequency shift. (a) Schematic diagram of the experimental setup. (b) Variation with frequency of the normalized intensity of the modulated pulse signal for a C2 rectangular meta-atom. The center frequency, amplitude, pulse period, and width of the modulated pulse signal are 10.5 GHz,  $-10 \text{ dBm}$ , 1.6 ms, and 0.4 ms, respectively. (c)–(e) RDE spectra of normalized intensity for C2 atom with clockwise angular velocity  $\Omega = 18 \times 2\pi$ ,  $27 \times 2\pi$ , and  $36 \times 2\pi$  rad/s. (f)–(h) RDE spectra of normalized intensity for C3 atom with clockwise angular velocity  $\Omega = 18 \times 2\pi$ ,  $27 \times 2\pi$ , and  $36 \times 2\pi$  rad/s.

C3 meta-atom is six times the rotation speed, which is consistent with our theoretical model. The above results indicate that the absolute value of the rotational Doppler frequency shift depends not only on the rotation speed but also on the rotational symmetry of the meta-atom. In addition, there are additional subpeaks that originate mainly from experimental imperfections, as any fluctuations in the wave due to unsteady rotation of the meta-atom lead to a modulation at the rotation frequency.

The variation with the rotational speed of the rotational frequency shift for C2 and C3 meta-atoms with a clockwise rotation direction is plotted in Figs. 4(a) and 4(b). The lines with blue and red dots correspond to the Doppler frequency shifts of the LCP and RCP components, respectively. More measurement results, for RDE spectrum analysis with different angular velocities and counterclockwise rotation, can be seen in Sec. S5 in the Supplemental Material [38]. It is found that the frequency shifts for the C2 and C3 meta-atoms show a linear relationship, with values of twice and

six times the rotational speed, respectively. A RDE with a higher rotational symmetry can be induced by a generalized PB phase using a meta-atom with a higher rotational symmetry, but this comes at the expense of efficiency and bandwidth [34]. For example, a C5 meta-atom with a periodic boundary in free space has been simulated, and the PB phase is ten times the rotation angle (see Sec. S6 in the Supplemental Material [38]). In contrast to full-size devices, a single meta-atom has minimal rotational inertia and size, enabling its potential application in integrated systems.

In addition, our scheme is easier to implement using a metallic material with high conductivity, and can be extended to metasurface devices with a periodic or aperiodic array of meta-atoms to arbitrarily and dynamically manipulate the wavefront of an electromagnetic wave by independently controlling the rotation angle of each element in real time. The scattering direction and angular momentum of the electromagnetic wave are determined

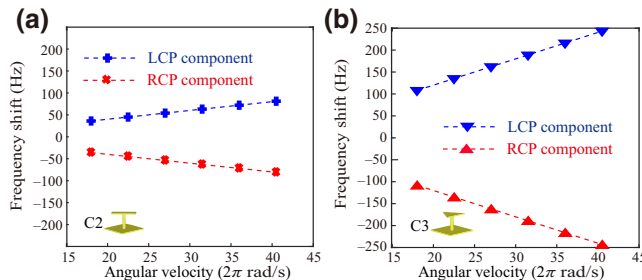


FIG. 4. Frequency shifts for C2 and C3 meta-atoms with different angular velocities and a clockwise rotation direction. (a) Doppler frequency shifts for the C2 meta-atom corresponding to the LCP and RCP components. (b) Doppler frequency shifts for the C3 meta-atom corresponding to the LCP and RCP components.

by the wavefront distribution, but the rotation angle for each meta-atom is equal to  $x(n)/f(n)$ , where  $x(n)$  is the local phase of the relative position, and  $f(n)$  is a function associated with the rotational symmetry  $n$ ;  $f(n) = 2n$  or  $n$  corresponds to odd or even rotational symmetry, respectively, of the meta-atom in a square lattice. This generalized PB phase depends on the coupling between adjoining elements. Therefore, there will be phase errors in the case of an aperiodic structure, but these can be ignored when the phase gradient is small. A rotationally symmetric meta-atom could produce frequency conversion under the condition of high-speed rotation, but the frequency shift is far smaller than the operating frequency of the meta-atom, and this does not affect the ability to manipulate electromagnetic waves by use of an arrangement of meta-atoms.

#### IV. CONCLUSION

In conclusion, we demonstrate both theoretically and experimentally that a multiple RDE can be induced by a single spinning meta-atom placed in a rectangular waveguide. In essence, the RDE originates from the time-varying PB phase of a symmetric meta-atom structure. Twofold and sixfold rotational Doppler shifts with respect to the rotational velocity are observed for meta-atoms with C2 and C3 rotational symmetry, respectively. The absolute rotational Doppler shift depends not only on the rotational speed but also on the rotational symmetry of the meta-atom structure. Thus, the rotational symmetry, which offers a degree of freedom for frequency-shift modulation, can amplify the rotational frequency shift in comparison with the traditional PB phase of a C2 meta-atom. The varying PB phase and multiple RDE induced by a single meta-atom observed here are different from the results in previous work on the PB phase induced by a periodic array metasurface with a full-size sample [39]. In contrast to full-size devices,

a single meta-atom with minimal rotational inertia and size enables a broad range of applications, especially in integrated systems. This work could open a path to inducing rotational Doppler shifts by use of the interaction of an electromagnetic wave with a single spinning meta-atom. It is expected that a higher-order generalized PB phase could be used to achieve a better rotation-detection system with high-precision performance in the future. In addition, our work may be extended to the infrared or visible range to achieve dynamic wavefront control by combining our technique with dynamic meta-atoms produced by means such as liquid crystals or nanomotors. This has possible applications in an OAM generator by employing a time-varying PB or OAM analyzer for measurement of orbital-angular-momentum modes based on the RDE.

#### ACKNOWLEDGMENTS

This work was supported by the National Natural Science Foundation of China (Grants No. 61975210, No. 62105338, and No. U20A20217). Jun Luo and Yuhui Wang contributed equally to this work.

- [1] C. Doppler, Ueber das farbige Licht der Doppelsterne und einiger anderer Gestirne des Himmels: Versuch einer das Bradley'sche Aberrations-Theorem als integrirenden Theil in sich schliessenden allgemeineren Theorie, Commission bei Borrosch & André **2**, 465 (1842).
- [2] A. Belopolsky, On an apparatus for the laboratory demonstration of the Doppler-Fizeau principle, *Astrophys. J.* **13**, 15 (1901).
- [3] D. L. Franklin, W. Schlegel, and R. F. Rushmer, Blood flow measured by Doppler frequency shift of back-scattered ultrasound, *Science* **134**, 564 (1961).
- [4] S. C. Jasper, Method of Doppler searching in a digital GPS receiver, U.S. Patent 4,701,934 (1987).
- [5] D. Atlas, R. Srivastava, and R. S. Sekhon, Doppler radar characteristics of precipitation at vertical incidence, *Rev. Geophys.* **11**, 1 (1973).
- [6] I. B. Birula and Z. B. Birula, Rotational Frequency Shift, *Phys. Rev. Lett.* **78**, 2539 (1997).
- [7] O. Korech, U. Steinitz, R. J. Gordon, I. S. Averbukh, and Y. Prior, Observing molecular spinning via the rotational Doppler effect, *Nat. Photonics* **7**, 711 (2013).
- [8] L. Fang, Z. Y. Wan, A. Forbes, and J. Wang, Vectorial Doppler metrology, *Nat. Commun.* **12**, 1 (2021).
- [9] W. H. Zhang, J. S. Gao, D. K. Zhang, Y. L. He, T. Z. Xu, R. Fickler, and L. X. Chen, Free-Space Remote Sensing of Rotation at the Photon-Counting Level, *Phys. Rev. Appl.* **10**, 044014 (2018).
- [10] D. Deng, H. Zhao, J. C. Ni, Y. Li, and C. W. Qiu, A phase-to-intensity strategy of angular velocity measurement based on photonic orbital angular momentum, *Nanophotonics* **11**, 865 (2022).

- [11] B. A. Garetz and S. Arnold, Variable frequency shifting of circularly polarized laser radiation via a rotating half-wave retardation plate, *Opt. Commun.* **31**, 1 (1979).
- [12] J. H. Deng, K. F. Li, W. Liu, and G. X. Li, Cascaded rotational Doppler effect, *Opt. Lett.* **44**, 2346 (2019).
- [13] M. P. Lavery, F. C. Speirits, S. M. Barnett, and M. J. Padgett, Detection of a spinning object using light's orbital angular momentum, *Science* **341**, 537 (2013).
- [14] M. P. Lavery, S. M. Barnett, F. C. Speirits, and M. J. Padgett, Observation of the rotational Doppler shift of a white-light, orbital-angular-momentum-carrying beam backscattered from a rotating body, *Optica* **1**, 1 (2014).
- [15] H. L. Zhou, D. Z. Fu, J. J. Dong, P. Zhang, D. X. Chen, X. L. Cai, F. L. Li, and X. L. Zhang, Orbital angular momentum complex spectrum analyzer for vortex light based on the rotational Doppler effect, *Light: Sci. Appl.* **6**, e16251 (2017).
- [16] J. Courtial, D. Robertson, K. Dholakia, L. Allen, and M. J. Padgett, Rotational Frequency Shift of a Light Beam, *Phys. Rev. Lett.* **81**, 4828 (1998).
- [17] G. Milione, S. Evans, D. Nolan, and R. R. Alfano, Higher Order Pancharatnam-Berry Phase and the Angular Momentum of Light, *Phys. Rev. Lett.* **108**, 190401 (2012).
- [18] G. X. Li, T. Zentgraf, and S. Zhang, Rotational Doppler effect in nonlinear optics, *Nat. Phys.* **12**, 736 (2016).
- [19] M. Khorasaninejad, W. T. Chen, R. C. Devlin, J. Oh, A. Y. Zhu, and F. Capasso, Metalenses at visible wavelengths: Diffraction-limited focusing and subwavelength resolution imaging, *Science* **352**, 1190 (2016).
- [20] J. B. Mueller, N. A. Rubin, R. C. Devlin, B. Groever, and F. Capasso, Metasurface Polarization Optics: Independent Phase Control of Arbitrary Orthogonal States of Polarization, *Phys. Rev. Lett.* **118**, 113901 (2017).
- [21] R. C. Devlin, A. Ambrosio, N. A. Rubin, J. B. Mueller, and F. Capasso, Arbitrary spin-to-orbital angular momentum conversion of light, *Science* **358**, 896 (2017).
- [22] X. H. Zhang, M. B. Pu, Y. H. Guo, J. J. Jin, X. Li, X. L. Ma, J. Luo, C. T. Wang, and X. G. Luo, Colorful metahologram with independently controlled images in transmission and reflection spaces, *Adv. Funct. Mater.* **29**, 1809145 (2019).
- [23] F. Zhang, M. B. Pu, P. Gao, J. J. Jin, X. Li, Y. H. Guo, X. L. Ma, J. Luo, H. L. Yu, and X. G. Luo, Simultaneous full-color printing and holography enabled by centimeter-scale plasmonic metasurfaces, *Adv. Sci.* **7**, 1903156 (2020).
- [24] Q. B. Fan, M. Z. Liu, C. Zhang, W. Q. Zhu, Y. L. Wang, P. C. Lin, F. Yan, L. Chen, H. J. Lezec, Y. Q. Lu, A. Agrawal, and T. Xu, Independent Amplitude Control of Arbitrary Orthogonal States of Polarization via Dielectric Metasurfaces, *Phys. Rev. Lett.* **125**, 267402 (2020).
- [25] M. F. Xu, Q. He, M. B. Pu, F. Zhang, L. Li, D. Sang, Y. H. Guo, R. Y. Zhang, X. Li, X. L. Ma, and X. G. Luo, Emerging long-range order from a freeform disordered metasurface, *Adv. Mater.* **34**, 2108709 (2022).
- [26] P. Georgi, C. Schlickriede, G. X. Li, S. Zhang, and T. Zentgraf, Rotational Doppler shift induced by spin-orbit coupling of light at spinning metasurfaces, *Optica* **4**, 1000 (2017).
- [27] F. Y. Yue, A. Aadhi, R. Piccoli, V. Aglieri, R. Macaluso, A. Toma, R. Morandotti, and L. Razzari, Rotational Doppler frequency shift from time-evolving high-order Pancharatnam-Berry phase: A metasurface approach, *Laser Photonics Rev.* **15**, 2000576 (2021).
- [28] Z. X. Liu, Y. Y. Liu, Y. G. Ke, J. X. Zhou, Y. C. Liu, H. L. Luo, and S. C. Wen, Geometric phase Doppler effect: When structured light meets rotating structured materials, *Opt. Express* **25**, 11564 (2017).
- [29] D. Ramaccia, D. L. Sounas, A. Alu, A. Toscano, and F. Bilotti, Phase-induced frequency conversion and Doppler effect with time-modulated metasurfaces, *IEEE Trans. Antennas Propag.* **68**, 1607 (2019).
- [30] B. Y. Liu, Y. J. He, S. W. Wong, and Y. Li, Multifunctional vortex beam generation by a dynamic reflective metasurface, *Adv. Opt. Mater.* **9**, 2001689 (2021).
- [31] B. Y. Liu, S. W. Wong, and Y. Li, Rotational Doppler effect by space-time-coding metasurfaces for nonreciprocal electromagnetic isolation, *Opt. Express* **29**, 24500 (2021).
- [32] B. Y. Liu, H. Giddens, Y. Li, Y. J. He, S. W. Wong, and Y. Hao, Design and experimental demonstration of Doppler cloak from spatiotemporally modulated metamaterials based on rotational Doppler effect, *Opt. Express* **28**, 3745 (2020).
- [33] D. G. Zhao, Y. T. Wang, K. H. Fung, Z. Q. Zhang, and C. T. Chan, Acoustic metamaterials with spinning components, *Phys. Rev. B* **101**, 054107 (2020).
- [34] X. Xie, M. B. Pu, J. J. Jin, M. F. Xu, Y. H. Guo, X. Li, P. Gao, X. L. Ma, and X. G. Luo, Generalized Pancharatnam-Berry Phase in Rotationally Symmetric Meta-atoms, *Phys. Rev. Lett.* **126**, 183902 (2021).
- [35] J. X. Cai, F. Zhang, M. B. Pu, Y. Chen, Y. H. Guo, T. Xie, X. D. Feng, X. L. Ma, X. Li, H. L. Yu, and X. G. Luo, All-metallic high-efficiency generalized Pancharatnam-Berry phase metasurface with chiral meta-atoms, *Nanophotonics* **11**, 1961 (2022).
- [36] G. X. Li, S. Zhang, and T. Zentgraf, Nonlinear photonic metasurfaces, *Nat. Rev. Mater.* **2**, 1 (2017).2058-8437
- [37] A. Belmonte and J. P. Torres, Optical Doppler shift with structured light, *Opt. Lett.* **36**, 4437 (2011).
- [38] See Supplemental Material at <http://link.aps.org/supplemental/10.1103/PhysRevApplied.19.044064> for further details of the theoretical, simulation, and experimental studies.
- [39] Q. Xu, X. Q. Su, X. Q. Zhang, L. J. Dong, L. F. Liu, Y. L. Shi, Q. Wang, M. Kang, A. Alù, S. Zhang, J. G. Han, and W. L. Zhang, Mechanically reprogrammable Pancharatnam-Berry metasurface for microwaves, *Adv. Photonics* **4**, 016002 (2022).